Multi-sourced data modelling of spatially heterogenous life-cycle carbon mitigation from installed rooftop photovoltaics: A case study in Singapore

Rui Zhu [a], Wing Sze Lau [b], Linlin You [c,*], Jinyue Yan [d], Carlo Ratti [e], Min Chen [f], Man Sing Wong [b,g], Zheng Qin [a]

[a] Institute of High Performance Computing (IHPC), Agency for Science, Technology and Research (A*STAR), 1 Fusionopolis Way, Singapore 138632, Republic of Singapore
[b] Department of Land Surveying and Geo-Informatics, The Hong Kong Polytechnic University, Hung Hom, Kowloon, Hong Kong, China
[c] School of Intelligent Systems Engineering, Sun Yat-Sen University, Shenzhen 518107, China
[d] Department of Building Environment and Energy Engineering, The Hong Kong Polytechnic University, Kowloon, Hong Kong, China
[e] Senseable City Laboratory, Department of Urban Studies and Planning, Massachusetts Institute of Technology, Cambridge, USA
[f] Key Laboratory of Virtual Geographic Environment (Ministry of Education of PRC), Nanjing Normal University, Nanjing, Jiangsu, China
[g] Research Institute for Land and Space, The Hong Kong Polytechnic University, Hung Hom, Kowloon, Hong Kong, China

HIGHLIGHTS

- Developed life-cycle-assessment integrated multi-sourced geospatial data model.
- Segmented rooftop PV areas using an advanced semantic segmentation model.
- Estimated installed PV electricity output using 3D solar estimation model.
- Suggested significant carbon mitigation potential from rooftop PVs in Singapore.
- Contributes to renewable energy transition and Information Geography development.

ARTICLE INFO

ABSTRACT

Accurately quantifying carbon mitigation of operational photovoltaics (PVs) influenced by dynamic geo-environment is crucial for developing suitable initiatives on renewable energy transition. However, previous studies made strong assumptions to avoid modelling spatial heterogeneity of carbon footprints or ignore weather and shadowing effects on PV electricity generation, making the estimated results unreliable and even causing false policymaking. To tackle this challenge, we developed a novel model coupling multi-sourced data modelling and life-cycle assessment to estimate spatially heterogenous carbon mitigation of all the operational rooftop PVs in an entire city. It is built by three hierarchal modules: (i) segmenting PV areas from high-resolution satellite imagery, by using Deep Solar PV Refiner, an advanced semantic segmentation network; (ii) estimating electricity generation in the segmented PV areas, by using a well-developed 3D solar irradiation model that considers the effects of land surface solar irradiation influenced by weather and shadowing effects produced by 3D buildings; (iii) quantifying carbon mitigation potential of PVs, by developing a spatial-aware life-cycle model to track the life-cycle carbon footprints of PVs from production, transportation, operation, to decommission. Investigating Singapore by 2020, we reveal that industrial, airport, and residential areas have the largest rooftop PV installation. We also suggest a carbon emission rate of 13.20 g-CO$_2$/kWh, a carbon payback time of 0.81 years, and an energy payback time of 0.94 years, showing an improved carbon mitigation capability compared to the past years. This study contributes to GIS data modelling and helps understand the geospatial characteristics of urban-scale PV carbon mitigation.

1. Introduction

1.1. Background

Many countries have adopted the Paris Agreement and the United Nations' Sustainable Development Goals to address global warming, with the aim of restricting global temperature increase to below 2 °C above pre-industrial levels and limiting the increase to 1.5 °C [1]. To achieve that, the governments and organizations around the globe are striving to transit to renewable energy such as solar energy to reduce greenhouse gas (GHG) emissions and air pollutions, making a sustainable alternative compared to fossil fuels [2].

It is believed that photovoltaic (PV) farming is one of the most promising ways to collect solar energy, which emits nearly zero carbon during the operation [3,4]. With this motivation, PV farming has become increasingly popular even in densely populated areas [5]. However, despite their potential as a sustainable energy solution for a resilient and carbon-free future, some argue that PV modules consume energy during their upstream and downstream phases, particularly during the manufacturing stage, which may offset the environmental benefits at certain degrees [6]. To accurately assess the environmental impacts and effectively assist and adjust policies for sustainability targets, quantifying carbon mitigation capability of the installed PV modules adapt to dynamic geo-environment is crucial.

Although statistics about PV area and installed capacity is available in some cities, it usually relies on manual data acquisition methods involving different public and private parties [7]. Although such methods are accurately, they are labour-intensive and time-consuming, making the collection unpractical when it comes to a large and fine scale. Additionally, these statistics usually lacks spatial information that makes it difficult to model spatiotemporal solar distribution affected by building shadow, consequently causing the estimated carbon reduction potential uncertain. To evaluate the environmental impacts of current PV systems to understand, refine, and improve a carbon neutral initiative, rapidly and accurately identifying installed PV area and location is greatly needed.

Meanwhile, carbon reduction potential was usually quantified by the difference of carbon emission factors between the current local grid and the alternative renewable energy [8,9]. This means that installed PV modules receiving different solar irradiation will have heterogenous electricity generation capability, resulting in various carbon reduction potential over time and space in cities. However, some studies estimated carbon reduction by disregarding the spatiotemporal heterogeneity with an assumption that all PV modules have the same power production [10,11]. Considering heterogenous distribution of PV potential affected by unstable weather, PV layouts, and building shadows, previous methods may cause large basis from the reality. Additionally, it is crucial to consider varying energy mix in different locations where PV systems are installed, which can result in significant differences in the mitigation of greenhouse gas emissions. Therefore, it is imperative to develop more sophisticated and location-specific approaches that account for these factors to obtain more accurate and reliable results.

Based on annual electricity generation of installed PV modules, life cycle assessment (LCA) can assess the environmental impacts of a product or system during the whole life cycle from raw material acquisition to the final disposal [12]. Even though many studies have investigated the LCA of PV systems, they either focused on large but coarse geographical scales [10,13] or simplified scenarios by ignoring operation and end-of-life management [14], which could overestimate the carbon reduction capability. Few have examined the carbon mitigation potential of distributed PV systems at the building level covering an entire city.

Regarding the three deficiencies as discussed above, this study aims to elaborately segment PV areas from high resolution satellite images, accurately estimate heterogeneously annual electricity generation of installed PV systems by considering the effects of unstable weather conditions and varying building shadows, and finally assess carbon reduction potential of existing PV modules by developing a low-cost, simple, and rapid LCA with geospatial modelling capability.

1.2. PV area segmentation

Conducting surveys on individual PV systems can be an arduous and time-consuming task, especially for PV systems on private properties that may not be easily accessible. To overcome this challenge, satellite imagery has been utilized to segment distributed PV areas in a large-scale, cost-effective, and efficient manner [15]. Since 2015, there has been significant interest in using satellite image-based approaches for PV area estimation. One study proposed a new detection approach that automatically identifies individual rooftop PV area from high-resolution satellite images to gather the system information such as installed capacity and energy generation, in a fast, reliable, and scalable way [16]. The results showed excellent locational detection performance; however, they did not provide pixel-level precision for PV area estimation. Subsequent study investigated two algorithms of Random Forest and Convolutional Neural Network (CNN), for PV array segmentation and found that CNN substantially outperformed Random Forest [17]. Similarly, another study proposed a ConvNet method to accurately extract solar panel locations and determine their spatial extent using aerial images [18].

In later studies, study in [19] presented a deep learning segmentation architecture that combines features of the MobileNet classification architecture and U-Net architecture, to optimize for efficient computation and achieved high recall (84.98%), precision (95.95%), and F1-score (90.13%). However, the segmented PV edges obtained from these algorithms were unsatisfactory in some situations. To solve these problems, one recent study in [20] developed a new model called TransPV by coupling U-Net and Vision Transformer, which respectively enables the combination of multi-level features and enhance the modelling of global context, resulting in refined PV segmentation with enriched feature representation.

Meanwhile, to evaluate the ability of various deep learning networks on PV area segmentation, study in [21] created a PV dataset using satellite images with spatial resolutions of 0.1, 0.3, and 0.8 m. The experiment showed that DeepLabv3+ outperformed U-Net and RefineNet. Even for the dataset at 0.8 m resolution, DeepLabv3+ performed well with Recall, Precision, and F1-score above 85%. Although DeepLabv3+ has proved highly effective, the PV edge detection from satellite imagery is still challenging because the foreground PV areas are easily impeded by background contexts having indistinguishable textures and colours [22]. To address this, one study in [23] introduced an advanced Deep-Labv3+ model that incorporates the Dual Attention Module (DAM) and PointRend Module (PRM), using a hybrid loss function (HLF) that combines cross-entropy loss, dice loss, and IoU loss functions to identify rooftop PV areas from satellite images. The model has been shown to improve the accuracy of PV area segmentation with a superior performance of a recall of 91.01%, a precision of 91.51%, and a F1-score of 91.26%, which provides a strong foundation for this study to accurately segment existing rooftop PV areas from satellite imagery and conduct an adaptive and reliable environmental assessment.

The use of public mapping services to evaluate urban environments is becoming increasingly popular [24], with Google Earth Satellite (GES) images being a valuable source of open-access data due to their wide coverage, frequent updates, and low acquisition costs [25]. With the

deep learning-based image semantic segmentation model, the barrier of large-scale surveying of PV installations can be addressed.

1.3. Solar irradiation and PV power estimation

Solar radiation databases are commonly used to estimate PV power, as demonstrated by [26], who used solar radiation maps from the Joint Research Centre of the European Commission to examine rooftop solar potential. Another study in [27] has estimated PV electricity generation and solar PV potential, by using solar radiation data obtained from sources such as NASA and atmosphere monitoring databases. However, relying solely on national solar radiation databases provides only an overall average radiation of the entire study area, rather than the radiation received by each PV module. As a result, the results obtained from such databases only give a rough estimation for the entire region.

Recently, novel studies have accurately estimated solar PV potential by integrated GIS and Remote Sensing techniques [28,29] and reliably evaluate techno-economic feasibility through geospatial analysis and planning [30–32]. While there are several GIS-based tools available for solar radiation and potential estimation that capture the complexities of the urban environment, one study argued that these tools often overlook crucial atmospheric parameters that affect solar radiation estimation [33]. Therefore, they employed a solar radiation model that accounts for atmospheric parameters to estimate solar PV potential in Netherlands, with a focus on calibrating the values of diffusivity and transmissivity.

Moreover, advancements in GIS technologies have led to studies on estimating rooftop PV capacity based on geospatial data. For example, study in [34] used LiDAR data to create a digital model of Auckland, which included terrain, building structures, and trees, as well as a solar radiation tool to compute the solar energy potential on each square meter of rooftop. Study in [29] used a GIS model to estimate solar radiation, improve the outcome with LiDAR and remote sensing images, and use regression analysis afterward. However, while LiDAR data offers rich information on both 2D images and height attributes, its acquisition cost may be a significant barrier when estimating solar PV potential on a large scale [27].

1.4. Life cycle assessment of carbon emissions from PV modules

Numerous studies have used the LCA methodology to investigate the environmental impacts of PV electricity generation [6,14,35], but few have focused on building-scale distributed PV systems adapting to the entire life cycle. Energy payback time (EPBT) and carbon payback time (CPBT) are two mostly used indicators. Although the production processes for PV modules are similar across countries, variations in emission amounts may occur. This makes it difficult to determine the exact emissions associated with a specific PV module and installed location. As early as 2005, study in [36] conducted a LCA on a 2.7 kWp distributed mono-crystalline silicon (mono-Si) solar PV system in Singapore.

Although PV systems provide significant benefits during their operational life, the production, transportation, and disposal of the components can have negative environmental impacts [37]. Therefore, it is important to conduct LCA to estimate the environmental impact of PV systems accurately. Study in [38] assessed the environmental impact by calculating primary energy demand and EPBT on multi-crystalline silicon (multi-Si) PV systems in China, with capacity of 200 Wp, cell efficiency of 16%, and lifespan of 25 years, considering only the production phase. The results range from 0.041 to 0.87 MJ/kWh and 2.2–6.1 years, respectively. Study in [14] conducted a LCA on a ground-mounted PV system, with 2017 kWh/m^2/year solar radiation and a conversion efficiency of 17.5%, in China, ignoring the operational process and end-of-life management, with EPBT calculated as 2.3 years. Another study conducted LCA by comparing three different roof-integrated p-type multi-Si PV technologies with efficiency ranging from 15.9% to 16.7% in Singapore, evaluating the entire value chain but neglecting the operational stage, transportation, and end-of-life management [39]. The authors used EPBT and GHG emissions as indicators of environmental impact, obtaining results ranging from 1.01 to 1.11 years and 20.9–30.2 g CO_2-eq/kWh, respectively.

1.5. Contributions

The major contribution of this study is developing a complete framework to evaluate the carbon mitigation potential of distributed PV systems at a city scale by integrating a semantic image segmentation model to segment installed PV areas from satellite imagery, adapting a rooftop solar irradiation estimation model to estimate annual PV electricity generation influenced by varying atmospheric conditions and building shadows, and developing a spatial-aware life-cycle model to accurately quantify PV carbon footprints. By comprehensively adapting GIS, remote sensing, deep learning, and LCA technologies, the framework can be easily generalized for other cities and the study contributes to understand the geospatial characteristics of urban-scale PV carbon mitigation.

The subsequent sections of the paper are organized as follows. Section 2 outlines the methodology used in the study, including the study area and datasets. Section 3 presents the experimental results and analysis. Section 4 introduces the discussion and Section 5 draws the conclusion.

2. Methodology

We propose a research framework that includes three main modules: deep learning-based PV area segmentation from satellite imagery, estimation of annual rooftop electricity generation from installed rooftop PVs, and LCA-based estimation of carbon mitigation potential (Fig. 1). The first module segments PV areas from high spatial resolution satellite images by using an advanced semantic segmentation network. The second module quantifies annual PV electricity, by coupling the segmented PV areas, historical weather that determines land-surface solar irradiation, and building rooftops with height attributes used to model shadowing effects. The third module evaluates PV impacts from the manufacturing stage to the end-of-life management of PV in terms of Cumulative Energy Demand, Carbon Emission Rate, EPBT, and CPBT.

2.1. Study area

The total electricity consumption in Singapore has increased from 50.8 TWh in 2020 to 53.5 TWh in 2021, a rise of 5.3% [40]. Meanwhile, Singapore receives abundant sunshine with an average annual solar irradiance of 1580 kWh/m^2/year [41], which indicates a significant PV potential to offset carbon emissions from traditional fuel-based electricity generation. Thus, the Government has demonstrated a commitment to promote PV deployment through various policies and funding schemes. This study investigated the entire territory of Singapore. The west areas marked in Fig. 2 were used to train, validate, and test the segmentation model, and the well-trained model was used for PV area segmentation in the entire territory.
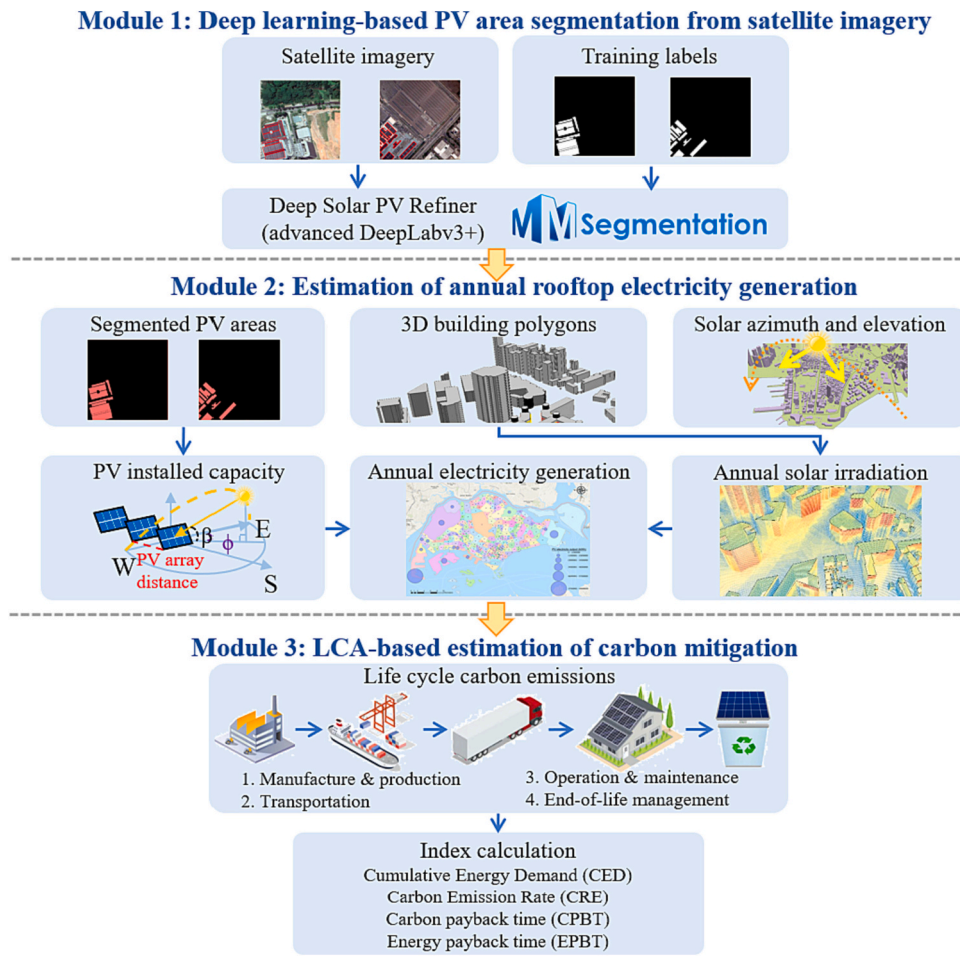
Fig. 1. Research framework for carbon reduction estimation.

2.2. Estimation of installed PV capacity

2.2.1. Semantic segmentation of PV areas

Deep Solar PV Refiner [23], an advanced DeepLabv3+, was used in this study for rooftop PV area segmentation from satellite images. The model integrated several advanced deep learning techniques, including *Parallel Connection of Separate ASPP and DAM*, *PointRend Module*, and *Hybrid Loss Function* (combining cross-entropy loss, dice loss, and IoU loss) to improve the accuracy of segmentation results. In addition, the network employed ResNeSt as the backbone, which allows it to capture both local and global contextual information while reducing computational cost. After segmentation, regularization based on a polyline compression algorithm was performed to polygonise and refine the boundaries of PV areas, which also removes interior rings occurring in some of the PV polygons.

2.2.2. Transfer learning

The accuracy of a model can be improved with a larger dataset. However, collecting a large dataset is time-consuming and resource intensive. Transfer learning and fine-tuning with a limited dataset has been a common training technique to improve the performance of a semantic segmentation model [22]. The experience and knowledge gained from previously trained model (i.e., Deep Solar PV Refiner) was repurposed to assist with the execution of new tasks in this study.

2.2.3. Installed PV capacity

Since Singapore is located near the equator, a tilted angle of 10–15° for PV panels is recommended to prevent raindrops and dust from obstructing the panels and reducing their efficiency. Thus, an average

angle of 10° was adopted for estimating PV areas segmented from the satellite imagery. On the other hand, all rooftops in this study were regarded as horizontal planes. The rooftop PV areas with a tilted angle were calculated in Eq. (1), where A_t is the area of solar PV with a tilted angle in m^2, A_S is the segmented PV area in m^2, and α is the tilted angle of solar PV panels in degree. Installed capacity refers to the maximum power generation of the installed PV system under optimal conditions as calculated in Eq. (2).

$$A_t = \frac{A_S}{cos\alpha} \tag{1}$$

$$Installed\ capacity = Product\ power \times A_t \tag{2}$$

2.3. Annual rooftop solar PV potential

2.3.1. Estimation of transmittivity and diffuse proportion

Cloud significantly affects land-surface solar radiation because it can scatter or absorb solar radiation, reducing the amount of direct radiation that reaches PV modules and causing fluctuations in solar power output [27]. Therefore, transmittivity and diffuse proportion were calculated in Eqs. (3) and (4) to quantify land-surface solar irradiation based on the cloud cover data [42], where M_t is the year average atmospheric transmittance, M_d is the year average diffuse proportion, P_{clear}, $P_{partlycloudy}$, and P_{cloudy} is the percentage of clear days, partly cloudy days, and cloudy days in each year, respectively.

$$M_t = 0.7 \times P_{clear} + 0.5 \times P_{partlycloudy} + 0.3 \times P_{cloudy} \tag{3}$$

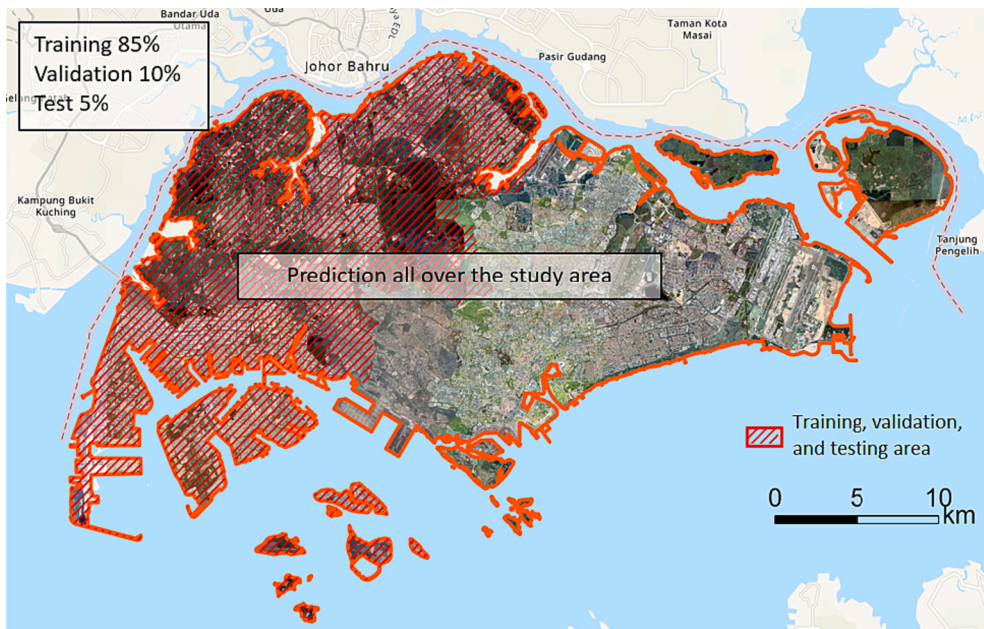$$M_d = 0.2 \times P_{clear} + 0.45 \times P_{partlycloudy} + 0.7 \times P_{cloudy} \tag{4}$$

Fig. 2. Study area covering the entire territory of Singapore.

2.3.2. Estimation of annual solar electricity output

The Area Solar Radiation toolset in ArcGIS Pro was used to estimate annual solar potential on building rooftops, which is one of the most professional solar estimation models that has been widely used in the previous study [43]. The toolset is a physical model that mathematically quantifies the effects of both cloud cover described by transmittivity and diffuse proportion and spatiotemporal shadow created by nearby buildings enriched with the height attribute. Furthermore, the total amount of electricity that a PV system can generate is simultaneously influenced by the PV area, unstable weather, spatiotemporal shadow, PV conversion efficiency, and performance ratio [43]. The equation is expressed in Eq. (5):

$$E_{pv} = A_t \times S \times r \times PR \tag{5}$$

where E_{pv} (kWh) is the annual solar electricity output of PVs; A_t (m^2) is the total area of the tilted PV modules in Eq. (1); S (kWh/m^2/yr) is the annual solar radiation received by PV modules affected by unstable weather and spatiotemporally heterogeneous shadow; r (%) is the PV conversion efficiency, and PR (%) is the performance ratio. In this study, 20% of PV conversion efficiency [44] and 75% of performance ratio was employed [43,45].

2.4. Life cycle assessment

The entire life cycle of a PV system consists of several stages, including manufacturing and production, transportation, operation and maintenance, and end-of-life processing of deconstruction, waste disposal, and recycling [46,47]. We assume that the lifetime of a PV system is 25 years [48,49] and we adapt two major types of PV modules in the model, which take about 61% for mono-Si and 39% for multi-Si, according to the latest statistics in Singapore [49]. The estimation is based on a standard 60-cell module with the size of 1 m × 1.6 m, which have a product power of 330 Wp for mono-Si and 280 Wp for multi-Si [44]. Fundamental parameters used in the estimation are summarized in Table 1.

For PV manufacturing and Balance-of-System (BOS) production, the energy input is almost the same while the corresponding carbon emission can be significantly different, mainly because of the varying energy structures in different countries. Thus, it is important to track the carbon footprints of PV modules to adapt to global PV trading. According to Climate Transparency (www.climate-transparency.org), we assume that the installed PV modules were produced in six countries of China, Canada, Germany, Japan, Singapore, and the USA, according to the latest market sharing of installed PV brands in Singapore. The corresponding carbon emissions for PV manufacturing were also summarized in Table 2, based on studies in [50,54].

For PV transportation, although it was suggested that the energy input and carbon emission for were small when compared to the manufacturing stage, uncontrollable uncertainty may be produced if it is only approximated by using a static index [39]. To address this issue, it is appropriate to infer that PV models were imported through ocean transport between container shipping ports and road transport between ports and installation sites.

The carbon emission from ocean transport by deep-sea containers is calculated in Eq. (6), where E_T is the carbon emission, V (tonnes) refers to the total transport volume, D (km) is the transport distance, and EF_T (kg-CO$_2$/t-km) denotes the average carbon emission factor [55]. The total transport volume used in this study was calculated by multiplying the total area of segmented PV (m^2) by the weight (kg/m^2), and the emission factor of ships or trucks subject to the transport distance. Based on the Sea Distance ORG (https://sea-distances.org/), the average shipping distance from the main ports of one country to Singapore are calculated, and the longest road transport distance from east to west of Singapore is 64 km. As a result, the emission factor and energy input of unit PV transportation is obtained in Table 3.

Table 1
Parameters for unit conversions and calculations.

Parameters	Values	Data source
Weight PV module (w)	15 kg/m^2	[51,52]
1 module (60-cell silicon PV module)	1.0 m × 1.6 m	
Product power of a mono-Si PV module	330 Wp	[44]
Product power of a multi-Si PV module	280 Wp	
Emission factor for ocean transport (EF_{OT})	5.7×10^{-3} kg-CO$_2$/t-km	
Emission factor for road transport (EF_{RT})	8.1×10^{-2} kg-CO$_2$/t-km	[53]
Energy input for ocean transport (EI_{OT})	5.29×10^{-2} t-km/kWh	[46]
Energy input for road transport (EI_{RT})	6.24×10^{-4} t-km/kWh	
Emission factor for decommission (EF_D)	0.4057 kg-CO$_2$/kWh	[54]

Table 2

Crucial parameters for PV manufacturing in six countries.

Country	Market sharing of PV systems in Singapore	National CO_2 emission factor (EF_M, kg-CO_2/kWh)
China	41.2%	0.5572
Canada	4.0%	0.1197
Germany	2.7%	0.3288
Japan	0.4%	0.4615
USA	8.0%	0.3580
Singapore	43.7%	0.4057

Table 3

Crucial parameters for PV transportation [44].

Category	Country	Transport distance (D, km)	Emission factor (EF_T, kg-CO_2/t-km)	Energy input (EI_T, MJ/m^2)
Ocean transport to Singapore	China	4142	0.3541	1.1832
	Canada	13,108	1.1207	3.7444
	Germany	15,729	1.3448	4.4931
	Japan	5378	0.4598	1.5363
	USA	14,203	1.2144	4.0572
Road transport	Singapore	64	0.0778	0.0022

$$E_T = V \times D \times EF_T \quad (6)$$

For PV maintenance, one replacement of inverter is assumed during the system life cycle, taking 0.1% of manufacturing input [56]. Because of the frequent rainfall in Singapore, cleaning of PV surfaces is not performed as often as necessary [39], and the cleaning process is neglected in this study.

For PV decommission, indirect carbon emission, which are generated outside of the manufacturing process but are necessary to deconstruct the PV system, is not always available. It includes the energy required to extract and process raw materials, as well as emissions generated from the disposal of waste during production [57]. As an estimation, indirect carbon emission from electricity consumption can be calculated in Eq. (7) [49], where E_D (kg-CO_2/m^2) is the indirect carbon emission, E_c (kWh/m^2) is the consumed electricity energy during the process by multiplying the energy conversion factor equalling 0.2778 kWh/MJ and the energy input of EI (MJ/m^2, Table 1), and EF_D (kg-CO_2/kWh, Table 1) is the emission factor from electricity generation.

$$E_D = E_c \times EF_D \quad (7)$$

For PV recycling, the carbon emission is −129 kg-CO_2/kWp for mono-Si and − 135 kg-CO_2/kWp for multi-Si [58]. By integrating the PV configurations summarized in Table 1, the carbon reduction potential can be easily obtained.

2.5. Estimation of carbon mitigation potential

2.5.1. Cumulative energy demand

Cumulative energy demand (CED) is used to measure the total amount of primary energy required to produce a specific amount of a product (i.e., the electricity to produce a unit PV module), considering all energy inputs throughout its entire life cycle [59]. Eq. (8) is designed for the scenario when different types of PV modules are installed in a city, where E_{Pi}, E_{Ti}, E_{Mi}, and E_{Di} represent the energy required for manufacturing, transporting, maintaining, and decommissioning a unit area of PV module, and R_i stands for the ratio of each PV type in the city.

$$CED = \sum_1^i (E_{Pi} + E_{Ti} + E_{Mi} + E_{Di}) \times R_i \quad (8)$$

2.5.2. Carbon emission rate

Carbon emission rate (CER) is a measure of the total carbon emission associate to a unit electricity generation from a PV during the entire life cycle [60]. According to the definition, the total carbon emission can be calculated in Eq. (9), where C_{Pi}, C_{Ti}, C_{Mi}, and C_{Di} represent the carbon emission associated with the corresponding stages for a PV module, and R_i stands for the ratio of such PV module in the city. Then, CER can be calculated in Eq. (10) [6], where E_A refers to the corresponding electricity output for a unit time, and t refers to the lifetime of PV system.

$$C_{total} = \sum_1^i (C_{Pi} + C_{Ti} + C_{Mi} + C_{Di}) \times R_i \quad (9)$$

$$CER = \frac{C_{total}}{E_A \times t} \quad (10)$$

2.5.3. Carbon reduction benefit

Life-cycle carbon reduction of a PV system is calculated in Eq. (11) [8] and the net carbon reduction benefit is defined in Eq. (12) [9]. Cr is the carbon reduction and Cr_{net} (kg-CO_2/m^2) is the net carbon reduction benefit from per m^2 of the PV system, E_A is the annual electricity generated per m^2 of the PV system, EF_c (kg-CO_2/kWh) is the carbon emission factor of the local grid, t denotes the lifespan of PV system, and C_{pv} (kg-CO_2/m^2) denotes the total carbon emissions per m^2 of PV system over its lifetime.

$$Cr = E_A \times EF_c \times t \quad (11)$$

$$Cr_{net} = Cr - C_{pv} \quad (12)$$

2.5.4. CPBT and EPBT

Carbon Payback Time (CPBT) refers to the period required for the PV system to offset the carbon emissions generated during its life cycle [61] and Energy Payback Time (EPBT) refers to the duration it takes for the solar PV system to generate an equivalent amount of energy that was used in its life cycle [6], which are calculated in Eqs. (13) and (14), respectively, where τ represents the energy conversion factor of converting primary energy into electrical energy in kWh/MJ as indicated in Table 1.

$$CPBT = \frac{C_{pv}}{E_A \times EF_c} \quad (13)$$

$$EPBT = \frac{CED}{E_A} \times \tau \quad (14)$$

2.6. Datasets

In this study, the GES images covering the entire territory of Singapore with spatial resolution of 0.8-m were retrieved in the end of 2020. The downloaded images were organized as 512 × 512 patches in 8 bits, consisting of 3 bands (RGB) in the Geo-TIFF format. As shown in Fig. 2, 30% of the total area from the Southwest and Northwest districts were extracted for labelling and utilized as the training (85%), validation (10%), and testing (5%) datasets, and the entire area is used for PV area segmentation. Building rooftop polygons enriched with the height attribute were acquired from Urban Redevelopment Authority. Historical data of daily cloud coverage percentage in years from 2020 to 2022 were acquired from World Weather Online (www.worldweatheronline.com), which was used to calculate M_t and M_d in Eqs. (3) and (4). Cloud cover taking 0–30%, 31–70%, and 71–100% is defined as clear sky, partly cloudy, and cloudy, respectively. Solar radiation elevation angles and azimuths were obtained from Weather Spark (www.weatherspark.com) for solar potential estimation.

3. Results

3.1. Segmented PV areas

Fig. 3 presents rooftop PV area segmentation results based on the satellite imagery, and Fig. 4 visualized the PV areas conversion from Raster to Polygon followed by boundary regularization and interior ring
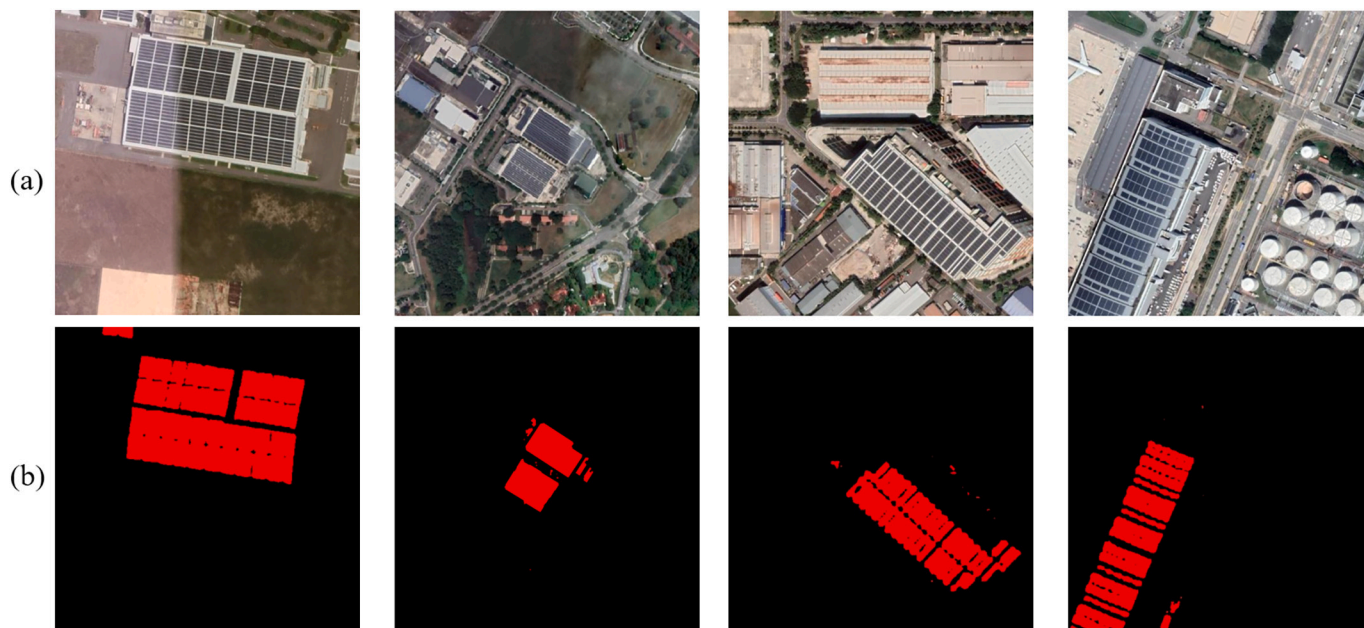
Fig. 3. Segmented rooftop PV areas. (a) GES images. (b) PV areas in the raster format.
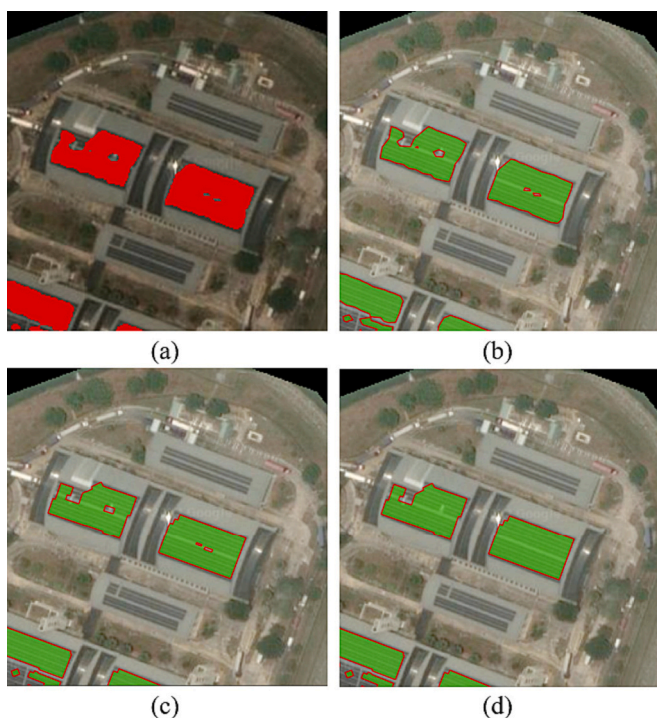

Fig. 4. Post-processing of segmented PV areas. (a) Raster format. (b) Polygon format. (c) PV boundary regularization. (d) Interior ring removal.

Table 4
Evaluation of the PV area segmentation using Deep Solar PV Refiner.

No.	Accuracy (%)	F1-score (%)	Precision (%)	Recall (%)
1	76.41	79.83	83.57	76.41
2	74.65	78.96	83.79	74.65
3	75.28	79.68	84.63	75.28
4	74.04	78.16	82.76	74.04
Mean	75.01	79.16	83.69	75.01
Post-processing	76.41	80.17	83.66	76.95

removal. Furthermore, 4-fold cross-validations were conducted to evaluate the performance of the trained models (Table 4). It shows that all experiments obtained similar results with tiny variations, and the mean scores are 75.01% for Accuracy, 79.16% for F1-score, 83.69% for Precision, and 75.01% for Recall. Based on the first trained model, the post-processing yielded true positive (TP), false positive (FP), false negative (FN), and true negative (TN) samples at 47.68%, 9.31%, 14.28%, and 28.73%, respectively. Consequently, the performance was enhanced, with Accuracy, F1-score, Precision, and Recall equalling to 76.41%, 80.17%, 83.66%, and 76.95%, respectively. The results are acceptable, according to a study that revealed accuracy distribution of rooftop PV area segmentation, influenced by various spatial resolutions [15]. Thus, we suggest it is effective for estimating the carbon reduction potential although the overall accuracy is not dramatically high.

The results have shown that rooftop PV systems in Singapore have a total installed area of approximately 1,859,949 m^2. By considering the product power of two types of PV modules (Table 1) and their market sharing (i.e., 61% for mono-Si and 39% for multi-Si), the total installed capacity is estimated to be 360.95 MWp. Notably, in this study, we investigated installed rooftop PVs by 2020, meaning that installed PVs on the ground and water surface were not counted. Thus, it is incomparable to the total 431.2 MWp by 2020 that includes all the sectors of private sector, town councils, public service agencies, and residential [62].

3.2. Spatial distribution patterns of installed rooftop PVs

In the spatial perspective, Fig. 5 shows that nearly all subzones in Singapore have installed rooftop PV systems. Specifically, Tuas Coast, a primarily industrial area in the southwest region, has the largest installed rooftop PV area, followed by Changi Airport in the northeast region. Meanwhile, it is noticeable that Lim Chu Kang and Western Water Catchment in the northwest and Jurong Island in the south have large size of rooftop PV areas. In comparison, rooftop PVs installed in Bukit Merah, the downtown area fulfilled by high density of tall buildings, are insignificantly large. In the thematic perspective, Fig. 6 reveals that the industrial, port & airport, and residential land use types take the largest PV installations, equalling 8.43×10^5 m^2 (45.33%), 2.58×10^5 m^2 (13.89%), and 1.57×10^5 m^2 (8.46%) PV areas, respectively. The two results are aligned with each other. It can be explained that the
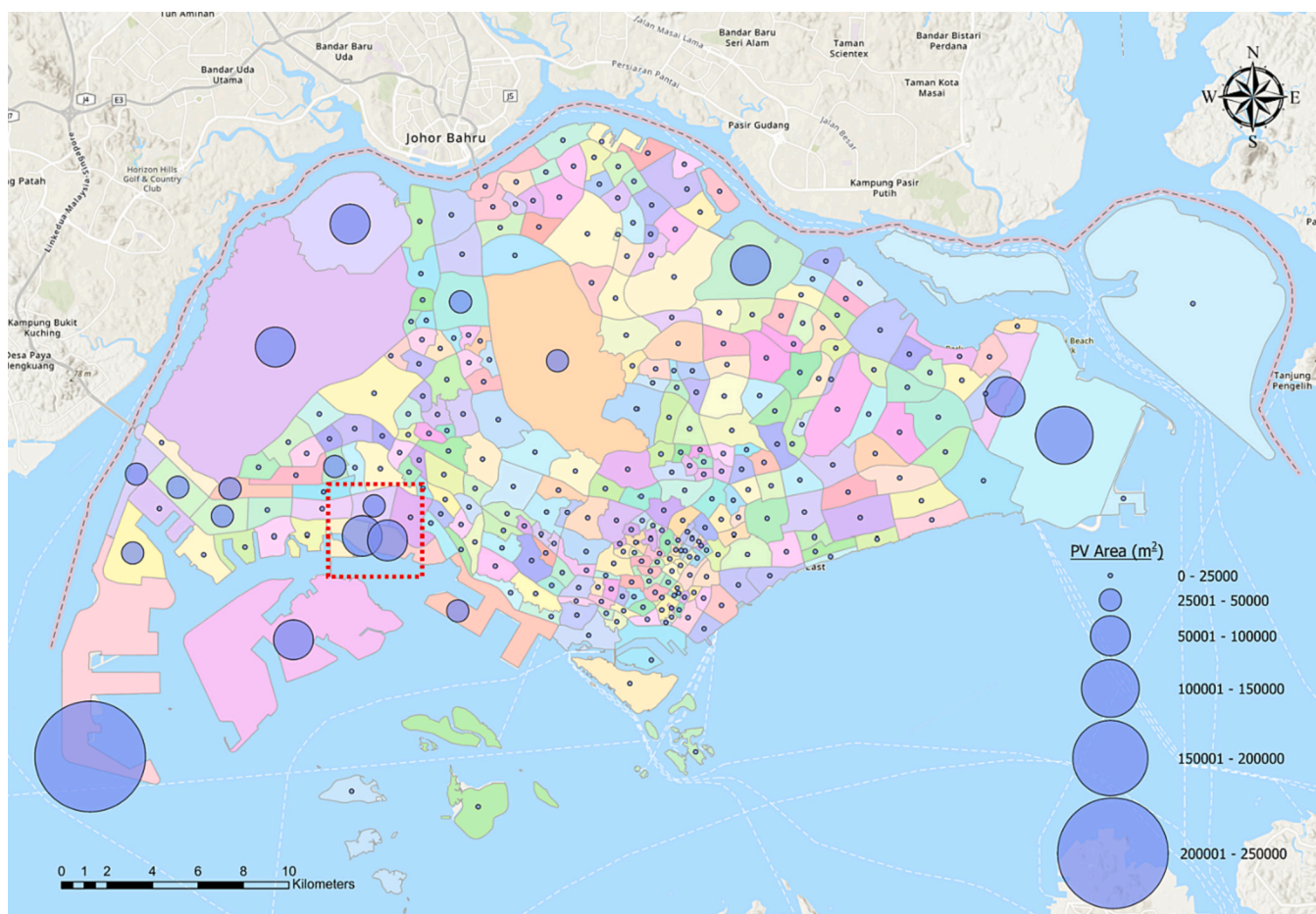
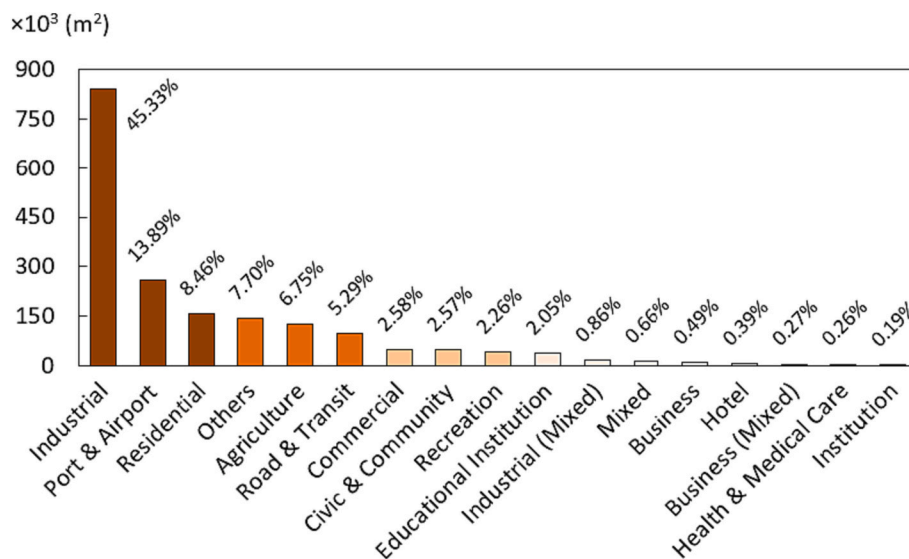Fig. 5. Installed rooftop PV area categorized by districts.

Fig. 6. Installed rooftop PV areas and the percentages categorized by land use types.

industrial (Tuas Coast) and port & airport (Changi Airport) areas have a great number of large and flat rooftops, suitable for PV installations and the Government has also established large initiatives to promote PV installations on residential buildings (e.g., HDB buildings built by the Government, home of 80% populations) and landed properties.

3.3. Annual electricity output of installed rooftop PVs

The average transmittivity (equalling 0.54) and diffuse proportion (equalling 0.39) over the three years from 2020 to 2022 were used for solar potential estimation (Section 2.3.1). Table 5 presents the average solar radiation on the installed rooftop PV surfaces throughout the year,

Table 5
Monthly average and annual solar irradiation in Singapore.

Month	Solar Irradiation (kWh/m^2)
Jan	125.69
Feb	122.70
Mar	149.13
Apr	140.88
May	134.48
Jun	122.77
Jul	131.32
Aug	142.72
Sep	150.15
Oct	136.57
Nov	123.57
Dec	120.84
Annual total	1600.82

with insignificant variation ranging from 120 to 150 kWh/m^2. As a result, Singapore receives an average annual solar radiation of 1600 kWh/m^2 for installed rooftop PVs according to our estimation, which is slightly higher than the figure (i.e., 1580 kWh/m^2) released by Energy Market Authority [41] and is almost 50% higher than that of many other countries [63]. This demonstrates that Singapore has abundant rooftop PV potential. Fig. 7 illustrates the monthly heterogeneous distribution of rooftop solar irradiation and its annual accumulation within a confined geographical area, featuring segmented PV areas depicted as semi-transparent blue polygons. Our analysis indicates that the shadowing effect on most PV areas is negligible because of the moderate building density and relatively uniform building heights. While a minority of PV areas receive comparatively low solar energy every month, the cumulative effect over the course of a year can be substantial.

By integrating the segmented rooftop PV areas with the heterogenous distribution of annual solar potential on rooftops, it allows us to estimate spatial-associated annual electricity generation. It is found that all rooftop PVs can generate electricity at 553,456,428 kWh/year, equivalent to 0.55 TWh/year, approximately. According to Statistical Review of World Energy 2022 [64], Singapore utilized renewable energy (including wind, geothermal, solar, biomass, and waste) and produced electricity at 1.0 TWh in 2020. This indicates that solar energy played an important role in energy transition in Singapore.

At this stage, we obtain a more meaningful and valuable estimation of annual electricity generation adaptive to the dynamic weather condition and 3D urban environment, comparing to the traditional estimation which only provides a static value about PV installed capacity. Fig. 8 presents that Tuas Coast, Changi Airport, and Jurong Island have the largest three PV installed capacities, which is consistent with the distribution pattern of rooftop PV areas as shown in Fig. 5. This can be explained by the fact that one of the largest rooftop solar installations in Singapore was completed in the Tuas area with an installed capacity of 4.7 MWp in 2019 and the project was expanded to 8.5 MWp in 2021. In 2022, a rooftop solar power system with an installed capacity of 3.5 MWp was also installed in the Changi Airport. In addition, the proportion of annual electricity generation is smaller than that of the installed capacity of rooftop PVs in the West Coast region, as shown in the red dashed rectangles in Fig. 5 and Fig. 8. This implies that the rooftop shadow effect is obvious in this region, where there is relatively high density of tall buildings.

3.4. Carbon mitigation potential

Based on the above results that provide crucial information of PV electricity production associated to specific urban locations, we can ultimately perform LCA of the energy input and carbon emission for a
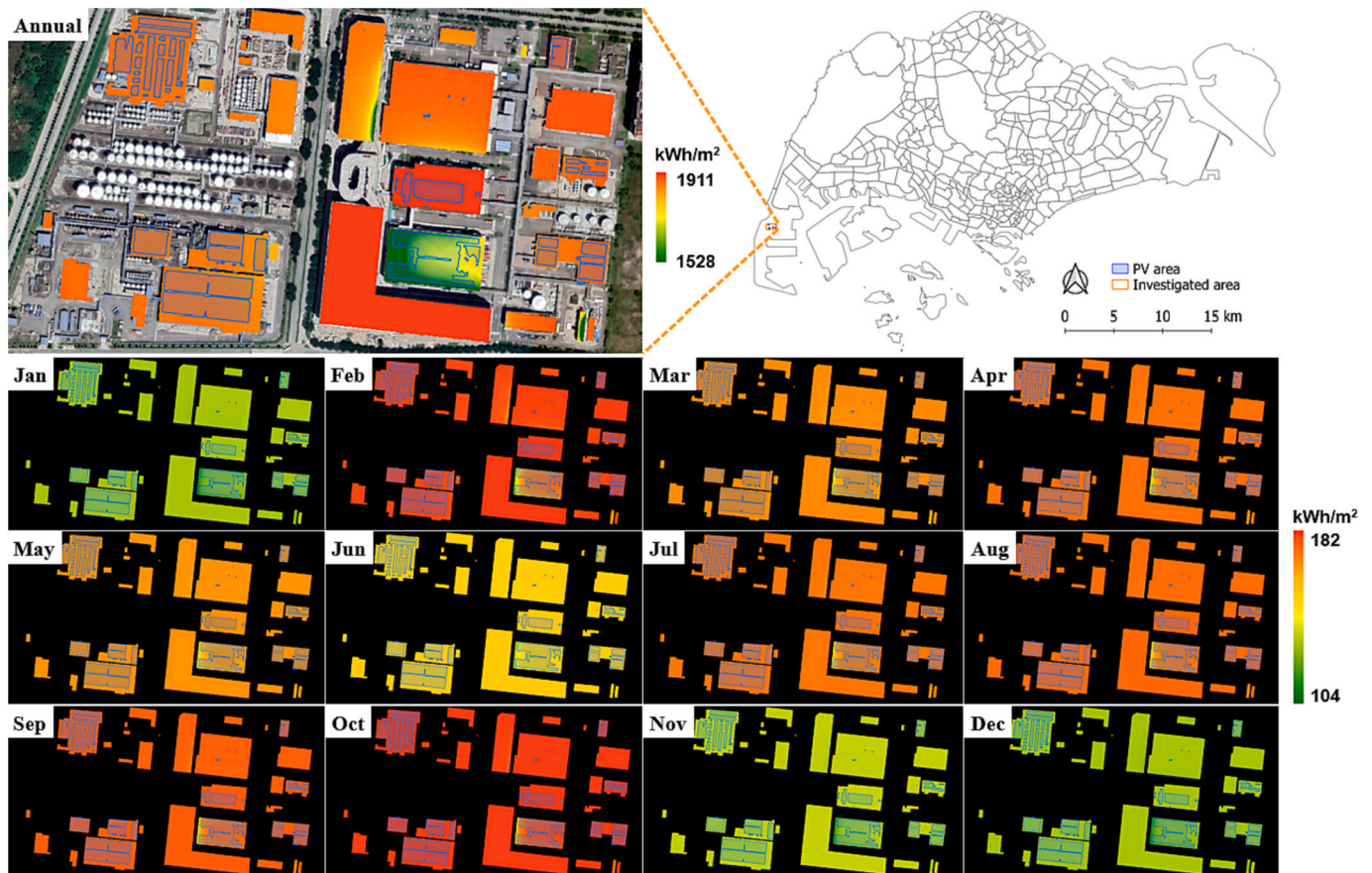

Fig. 7. Detailed visualization of spatiotemporal distribution of rooftop solar irradiation.
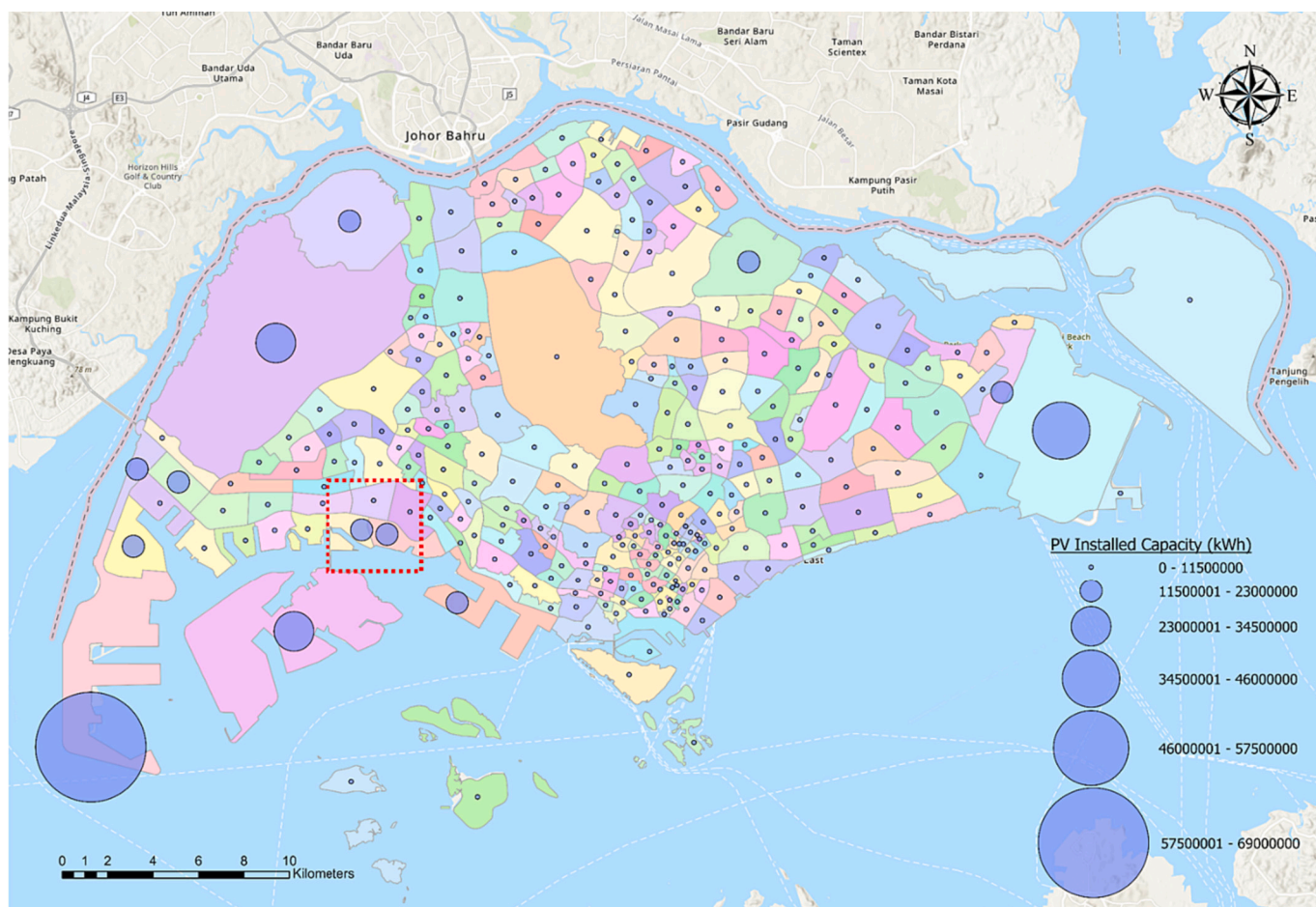
Fig. 8. Annual electricity output of installed rooftop PV categorized by districts.

Table 6
Energy input during the PV life cycle.

Phase	Source	Energy input	
		EI for mono-Si PV (MJ/m^2)	*EI* for multi-Si PV (MJ/m^2)
Manufacturing	PV module and BOS	822.2595	628.5894
Ocean transport	From China	1.1832	
	From USA	4.0572	
	From Canada	3.7444	
	From Germany	4.4931	
	From Japan	1.5363	
Road transport	In Singapore	0.0022	
Maintenance	Inverter replacement	0.8223	0.6286
Decommissioning	Deconstruction and disposal	262.50	250.00

Table 7
Carbon emission during the PV life cycle.

Phase	Source	Emission factor	
		EF (kg-CO$_2$/m^2) for mono-Si PV	*EF* (kg-CO$_2$/m^2) for multi-Si PV
Manufacturing	China	127.2777	97.2995
	USA	81.7757	62.5147
	Canada	27.3423	20.9023
	Germany	75.1057	57.4158
	Japan	105.4175	80.5881
	Singapore	92.6715	70.8442
Ocean transport	From China	0.3541	
	From USA	1.2144	
	From Canada	1.1207	
	From Germany	1.3448	
	From Japan	0.4598	
Road transport	In Singapore	0.0778	
Maintenance	Inverter replacement	0.1273	0.0973
Decommissioning	Deconstruction and disposal	29.5847	28.1759
Recycling	Reuse of PV cells	−26.6063	−23.6250

unit PV area. Table 6 demonstrates that PV manufacturing contributes to the largest energy input, taking 75% and 70% of the total energy consumption for mono-Si PV and multi-Si PV, respectively. Although the shipping distances sailing from the five countries to Singapore are significantly long, the energy input for ocean transport only takes a small proportion, suggesting considerably low-energy consumption. Furthermore, energy input for road transport is even ignorable since the road transportation distance in Singapore is rather short. Table 7 unravels large variation of carbon emission in the six countries for PV manufacturing. Specifically, China corresponds to the largest carbon emission as high as 127 kg-CO$_2$/m^2 for mono-Si and 97 kg-CO$_2$/m^2 for multi-Si, while Canada has the smallest carbon emission less than 30 kg-CO$_2$/m^2 for both types of PVs. This is mainly caused by various national energy structures. It is also revealed that carbon emission of ocean

transport from five countries is insignificant, which only takes a tiny proportion in a range of 0.27–3.54% for mono-Si PV and 0.35–4.19% for multi-Si PV out of the total carbon emission. Meanwhile, recycling can almost offset carbon emissions produced by decommissioning.

The above modelling suggested the total rooftop PV area and the corresponding installed capacity are 1,859,949 m^2 and 360.95 MWp, which can produce an annual electricity at 0.5535 TWh equivalent to 297.57 kWh/m^2. By integrating the results derived in Tables 6 and 7, the

Table 8
Summary of all important estimations.

No.	Parameter	Value	Unit
1	Total rooftop PV area	1,859,949	m^2
2	Total installed rooftop PV capacity	360.95	MWp
3	Total annual electricity output	0.5535	TWh
4	Annual electricity output per unit area	297.57	kWh/m^2
5	Life-cycle Energy Input Factor	1006.19	MJ/m^2
6	Life-cycle Carbon Emission Factor	98.18	kg-CO$_2$/m^2
7	Net Carbon Reduction Benefit	2919.87	kg-CO$_2$/m^2
8	Total Carbon Reduction Benefit	5,430,819.69	tonne
9	Carbon Emission Rate (CER)	13.20	g-CO$_2$/kWh
10	Carbon Payback Time (CPBT)	0.81	year
11	Energy Payback Time (EPBT)	0.94	year

life-cycle Energy Input Factor and Carbon Emission Factor are 1006.19 MJ/m^2 and 98.18 kg-CO$_2$/m^2 (Table 8). Furthermore, by calculating the difference of *reduced* carbon emission equivalent to the life-cycle electricity generation and *produced* carbon emission for a life-cycle unit PV, the Net Carbon Reduction Benefit is derived and equals 2919.87 kg-CO$_2$/m^2. This corresponds to a significant Total Carbon Reduction Benefit (i.e., carbon reduction of all existing rooftop PVs) at 5,430,819.69 t. Based on the totally reduced carbon reduction and electricity generation, the Carbon Emission Rate (CER) is calculated, which equals 13.20 g-CO^2/kWh. As a result, The Carbon Payback Time (CPBT) is 0.81 year and Energy Payback Time (EPBT) is 0.94 year only (Table 8).

A similar study which also investigated in Singapore in 2018 stated that the CER was 30.2, 29.2, and 20.9 g-CO$_2$/kWh for three types of multi-Si PVs with different technologies, and the EPBT was 1.01–1.11 years [39]. Although one study conducted in 2019 suggested that the CPBT and EPBT were 1.86–9.16 years and 1.98–4.58 years, respectively, in Morocco and Portugal [65], other studies found that it was shorter than one year for CPBT (i.e., 0.39 years [37,66], and 0.884 years [67], and 143 days in Delhi, India [68]) and EPBT (i.e., 0.7, 0.83, and 0.9 years for Brazil, US, and China, respectively [49] and 0.68 and 0.92 years based on the equipment manufacturers' estimation [69]). The shorter periods derived from our study are mainly because of (i) refined estimation of annual electricity generation from existing PV panels to replace the conventionally installed capacity-based estimation, and (ii) considerably improved energy structure of the two major PV manufacturing countries – China and Singapore.

4. Discussion

Our results imply that Singapore, as a city-scale state, has a strong capability in carbon mitigation derived from installed rooftop PVs. This is based on the evidence that CER achieves almost a 50% reduction, and both CPBT and EPBT become significantly shorter compared to previous studies conducted roughly five years ago in Singapore. There are three major reasons to get a noticeable improvement of the carbon mitigation potential. Firstly, both China and Singapore experienced improvements in their energy structures, resulting in smaller national carbon emission factors for electricity generation. Additionally, the two countries manufactured approximately 84% of the PVs installed in Singapore. Secondly, rather than relying on static installed capacity figures, we advanced the estimation by simulating annual PV electricity generation, accounting for the spatiotemporally dynamic and heterogeneous solar conditions, including explicit PV locations, varying weather conditions, and dynamic shadowing effects. Thirdly, we developed a model that encompasses complete life-cycle carbon emissions, considering the influence of multiple PV providers, global supply chains, and various types of PV cells.

Our results highlight an environmental inequality concern. We suggest Singapore can obtain a large amount of carbon reduction during the whole life cycle of existing rooftop PVs. However, this is contingent on

the fact that 56.3% of the PVs were imported from other countries, with 41.2% originating from China, the largest PV exporter with the highest carbon emission factor among the five countries. Although China has significantly improved energy structure during the past few years, the result still implies that the cumulative carbon emissions from PV manufacturing in China could be significant. Given these considerations, the continuous improvement of the energy structure, adaptive to global supply chains and coupled with an increased reliance on renewable energy sources, becomes crucial for sustainable development.

The framework presented in this study is scalable and can be applied to any other cities. The major reasons are that advanced semantic segmentation models (including, but not limited to, Deep Solar PV Refiner) with transfer learning can be employed to accurately identify PV areas and locations, GES images are publicly accessible, and rooftop solar PV potential can be estimated using well-established Area Solar Radiation models. Since Singapore has flat terrain, this study relied solely on building heights for rooftop solar potential estimation. For a steep and elevated city like Hong Kong, a Digital Surface Model or a Digital Elevation Model may be integrated. Once statistics about the market share of PV providers and PV types are obtained, all information can be integrated into the advanced LCA framework with a high degree of accuracy.

The semantic segmentation correctly identified 76.41% of PV samples (i.e., Accuracy) while mistakenly identified 9.31% of PV samples (proportion of FP) and 14.28% of non-PV samples (proportion of FN). This implies that 9.31% of FP and 9.31% of FN precisely offset each other on annual PV electricity generation to a large extent. This is because rooftop PV areas belonging to either FP or FN are generally located at solar-abundant locations in Singapore. Consequently, the 4.97% residual PV samples (the difference of FN and FP), which should represent actual PV areas but have not been segmented successfully, will cause directly adverse effects. As positive predictions encompass 56.99% of PV samples (the sum of TP and FP), the 4.97% residual PV samples will likely introduce uncertainty into accumulated statistics, with an upper limit of 8.72%, such as the total rooftop PV area. Nevertheless, the uncertainty has insignificant effects on carbon mitigation potential estimation, such as the key figures of CER, CPBT, and EPBT presented in Table 8. This is because the estimation was based on the unit area, not accumulated areas. Additionally, we conducted mathematically significant analyses to quantify annual averaged PV electricity generation per unit area by integrating all the segmented rooftop PV areas and accurate solar potential distribution, and we created carbon emission profiles by tracing the global supply chains.

This study may produce certain discrepancy or uncertainty because of the resolution of LCA analysis and the spatial resolution of GIS data. First, we assumed that PV modules were manufactured in six countries according to their PV brands and market shares. This means that some PVs might be manufactured in other countries, which, however, only took around 14% PVs not coming from China and Singapore. Second, we assumed all rooftop PVs were installed with a title angle of 10°, which is widely applied in Singapore. Although this assumption may create certain bias to reality, the effects should be considerably small since exceptional cases typically occur at only a few landed properties. Third, we assumed a static PV conversion efficiency. This means that the conversion efficiency was not reduced by urban thermal environment and had no degradation over the years. Future work can improve the model by integrating these effects into the spatiotemporal estimation and analyse the carbon mitigation capacity when PV modules are installed on new rooftops amidst the ongoing urbanization process in the future.

5. Conclusion

In conclusion, this study developed a geospatial-enriched life-cycle assessment model to estimate city-scale carbon mitigation capability of existing rooftop PV systems. The results reveal that, at the city scale,

installed rooftop PVs in Singapore have a strong carbon reduction capability. The model is scalable and generalizable to other cities for rapid, complete, and cost-effective assessment, which can facilitate policymakers to review and adjust their strategies towards sustainability targets. This study contributes to GIS spatiotemporal data modelling and the transition to renewable energy.

CRediT authorship contribution statement

Rui Zhu: Writing – review & editing, Writing – original draft, Visualization, Validation, Supervision, Methodology, Formal analysis, Conceptualization. **Wing Sze Lau:** Writing – original draft, Visualization, Software, Methodology, Formal analysis, Data curation. **Linlin You:** Writing – review & editing, Supervision, Methodology, Conceptualization. **Jinyue Yan:** Writing – review & editing, Supervision, Investigation. **Carlo Ratti:** Writing – review & editing, Supervision, Investigation. **Min Chen:** Writing – review & editing, Supervision, Investigation. **Man Sing Wong:** Writing – review & editing, Supervision, Funding acquisition. **Zheng Qin:** Writing – review & editing, Supervision, Investigation.

Declaration of competing interest

The authors declare that they have no known competing financial interests or personal relationships that could have appeared to influence the work reported in this paper.

Data availability

Data will be made available on request.

Acknowledgment

References

[1] McGlade C, Ekins P. The geographical distribution of fossil fuels unused when limiting global warming to 2°C. Nature 2015;517:187–90.

[2] Zhu R, Kwan MP, Perera ATD, et al. GIScience can facilitate the development of solar cities for energy transition. Adv Appl Energy 2023;10:100129.

[3] Schmittera P, Kibret KS, Lefored N, Barron J. Suitability mapping framework for solar photovoltaic pumps for smallholder farmers in sub-Saharan Africa. Appl Energy 2018;94:41–57.

[4] Zhang Z, Chen M, Zhong T, Zhu R, et al. Carbon mitigation potential afforded by rooftop photovoltaic in China. Nat Commun 2023;14:2347.

[5] Brito MC, Freitas S, Guimarães S, Catita C, Redweik P. The importance of facades for the solar PV potential of a Mediterranean city using LiDAR data. Renew Energy 2017;111:85–94.

[6] Peng J, Lu L, Yang H. Review on life cycle assessment of energy payback and greenhouse gas emission of solar photovoltaic systems. Renew Sustain Energy Rev 2013;19:255–74.

[7] Boulahia M, Djiar KA, Amado M. Combined engineering—statistical method for assessing solar photovoltaic potential on residential rooftops: case of Laghouat in central southern Algeria. Energies 2021;14(6):1626.

[8] Amine Deriche M, Hafaifab A, Mohammedia K. EPBT and CO_2 emission from solar PV monocrystaline silicon. In: 2018 International Conference on Applied Smart Systems (ICASS); 2018. p. 1–3.

[9] Xi C, Wang D, Cao SJ. Impacts of trees-grass area ratio on thermal environment, energy saving, and carbon benefits. Urban Clim 2023;47:101393.

[10] Taborianski VM, Pacca SA. Carbon dioxide emission reduction potential for low income housing units based on photovoltaic systems in distinct climatic regions. Renew Energy 2022;198:1440–7.

[11] Park HS, Jeong K, Hong T, Ban C, Koo C, Kim J. The optimal photovoltaic system implementation strategy to achieve the national carbon emissions reduction target in 2030: focused on educational facilities. Energ Buildings 2016;119:101–10.

[12] Muteri V, Cellura M, Curto D, Franzitta V, Longo S, Mistretta M, et al. Review on life cycle assessment of solar photovoltaic panels. Energies 2020;13(1):252.

[13] Guo X, Dong Y, Ren D. CO_2 emission reduction effect of photovoltaic industry through 2060 in China. Energy 2023;269:126692.

[14] Wu P, Ma X, Ji J, Ma Y. Review on life cycle assessment of energy payback of solar photovoltaic systems and a case study. Energy Procedia 2017;105:68–74.

[15] Li P, Zhang H, Guo Z, Lyu S, Chen J, Li W, et al. Understanding rooftop PV panel semantic segmentation of satellite and aerial images for better using machine learning. Adv Appl Energy 2021;4:100057.

[16] Malof JM, Hou R, Collins LM, Bradbury K, Newell R. Automatic solar photovoltaic panel detection in satellite imagery. In: 2015 International Conference on Renewable Energy Research and Applications; 2015. p. 1428–31.

[17] Malof JM, Collins LM, Bradbury K, Newell RG. A deep convolutional neural network and a random forest classifier for solar photovoltaic array detection in aerial imagery. In: 2016 IEEE International Conference on Renewable Energy Research and Applications; 2016. p. 650–4.

[18] Yuan J, Yang HHL, Omitaomu OA, Bhaduri BL. Large-scale solar panel mapping from aerial images using deep convolutional networks. In: 2016 IEEE International Conference on Big Data; 2016. p. 2703–8.

[19] Wani MA, Mujtaba T. Segmentation of satellite images of solar panels using fast deep learning model. Int J Renew Energy Res 2021;11(1):31–45.

[20] Guo Z, Lu J, Chen Q, Liu Z, Song C, Tan H, et al. TransPV: refining photovoltaic panel detection accuracy through a vision transformer-based deep learning model. Appl Energy 2024;355:122282.

[21] Jiang H, Yao L, Lu N, Qin J, Liu T, Liu Y, et al. Multi-resolution dataset for photovoltaic panel segmentation from satellite and aerial imagery. Earth Syst Sci Data 2021;13(11):5389–401.

[22] Qian Z, Chen M, Zhong T, Zhang F, Zhu R, et al. A detail-oriented deep learning network for refined delineation of roof structure lines using satellite imagery. Int J Appl Earth Observ Geoinform 2022;107:102680.

[23] Zhu R, Guo D, Wong MS, Qian Z, et al. Deep solar PV refiner: an advanced deep learning network for photovoltaic area segmentation from satellite imagery. Int J Appl Earth Observ Geoinform 2023;116:103134.

[24] Liang J, Gong J, Li W. Applications and impacts of Google earth: a decadal review (2006–2016). ISPRS J Photogr Remote Sens 2018;146:91–107.

[25] Qi F, Wang Y. A new calculation method for shape coefficient of residential building using Google earth. Energ Buildings 2014;76:72–80.

[26] Bergamasco L, Asinari P. Scalable methodology for the photovoltaic solar energy potential assessment based on available roof surface area: application to Piedmont region (Italy). Solar Energy 2011;85(5):1041–55.

[27] Zhong T, Zhang Z, Chen M, Zhang K, et al. A city-scale estimation of rooftop solar photovoltaic potential based on deep learning. Appl Energy 2021;298:117132.

[28] Jiang H, Zhang X, Yao L, Lu N, Qin J, Liu T, et al. High-resolution analysis of rooftop photovoltaic potential based on hourly generation simulations and load profiles. Appl Energy 2023;348:121553.

[29] Jiang H, Yao L, Lu N, Qin J, Liu T, Liu Y, et al. Geospatial assessment of rooftop solar photovoltaic potential using multi-source remote sensing data. Energy AI 2022;10:100185.

[30] Bhanja R, Roychowdhury K. A spatial analysis of techno-economic feasibility of solar cities of India using electricity system sustainability index. Appl Geogr 2023; 154:102893.

[31] Fournier ED, Federico F, Cudd R, Pincetl S. Building an interactive web mapping tool to support distributed energy resource planning using public participation GIS. Appl Geogr 2023;152:102877.

[32] Mentis D, Andersson M, Howells M, Rogner H, Siyal S, Broad O, et al. The benefits of geospatial planning in energy access – a case study on Ethiopia. Appl Geogr 2016;72:1–13.

[33] Kausika BB, van Sark WG. Calibration and validation of ArcGIS solar radiation tool for photovoltaic potential determination in the Netherlands. Energies 2021;14(7): 1865.

[34] Suomalainen K, Wang V, Sharp B. Rooftop solar potential based on LiDAR data: bottom-up assessment at neighbourhood level. Renew Energy 2017;111:463–75.

[35] Gerbinet S, Belboom S, Léonard A. Life cycle analysis (LCA) of photovoltaic panels: a review. Renew Sustain Energy Rev 2014;38:747–53.

[36] Kannan R, Leong KC, Osman R, Ho HK, Tso CP. Life cycle assessment study of solar PV systems: an example of a 2.7 kWp distributed solar PV system in Singapore. Solar Energy 2006;80(5):555–63.

[37] Grant C, Garcia J, Hicks A. Environmental payback periods of multi-crystalline silicon photovoltaics in the United States – How prioritizing based on environmental impact compares to solar intensity. Sustain Energy Technol Assess 2020;39:100723.

[38] Fu Y, Liu X, Yuan Z. Life-cycle assessment of multi-crystalline photovoltaic (PV) systems in China. J Clean Prod 2015;86:180–90.

[39] Luo W, Khoo YS, Kumar A, Low JSC, et al. A comparative life-cycle assessment of photovoltaic electricity generation in Singapore by multicrystalline silicon technologies. Solar Energy Mater Solar Cells 2018;174:157–62.

[40] Energy Market Authority. Chapter 3: Energy Consumption. 2022.

[41] Energy Market Authority. What is the potential of solar energy in Singapore?. 2023.

[42] Huang S, Rich PM, Crabtree RL, Potter CS, Fu P. Modeling monthly near-surface air temperature from solar radiation and lapse rate: application over complex terrain in Yellowstone National Park. Phys Geogr 2008;29(2):158–78.

[43] Zhu R, Wong MS, Kwan MP, Chen M, Santi P, Ratti C. An economically feasible optimization of photovoltaic provision using real electricity demand: A case study in New York city. Sustainable Cities and Society; 2022. p. 103614.

[44] Aberle A, Duttagupta S, Khoo YS, Kumar A, et al. Update of the Solar PV Roadmap for Singapore. 2020.

[45] Ye Y, Zhu R, Yan J, Lu L, et al. Planning the installation of building-integrated photovoltaic shading devices: a GIS-based spatiotemporal analysis and optimization approach. Renew Energy 2023;216:119084.

[46] Ali A, Koch TW, Volk TA, Malmsheimer RW, et al. The environmental life cycle assessment of electricity production in New York state from distributed solar photovoltaic systems. Energies 2022;15(19):7278.

[47] Mulazzani A, Eleftheriadis P, Leva S. Recycling c-Si PV modules: a review, a proposed energy model and a manufacturing comparison. Energies 2022;15(22):8419.

[48] Akinyele DO, Rayudu RK. Techno-economic and life cycle environmental performance analyses of a solar photovoltaic microgrid system for developing countries. Energy 2016;109:160–79.

[49] Yıldız G, Çalış B, Gürel AE, Ceylan İ. Investigation of life cycle CO_2 emissions of the polycrystalline and cadmium telluride PV panels. Environ Nanotechnol Monitor Manag 2020;14:100343.

[50] National Solar Repository of Singapore. PV system characteristics. 2023.

[51] Nabil T, Mansour TM. Augmenting the performance of photovoltaic panel by decreasing its temperature using various cooling techniques. Results Eng 2022;15:100564.

[52] Song G, Lu Y, Liu B, Duan H, Feng H, Liu G. Photovoltaic panel waste assessment and embodied material flows in China, 2000-2050. J Environ Manage 2023;338:117675.

[53] Smart Freight Centre. Calculating GHG transport and logistics emissions for the European Chemical Industry. 2021.

[54] National Climate Change Secretariat. Energy reset: a more environmentally friendly method to power our nation. 2023.

[55] Asian Development Bank. Guidelines for estimating greenhouse gas emissions of Asian Development Bank projects: additional guidance for transport projects. 2016.

[56] Hou G, Sun H, Jiang Z, Pan Z, Wang Y, Zhang X, et al. Life cycle assessment of grid-connected photovoltaic power generation from crystalline silicon solar modules in China. Appl Energy 2016;164:882–90.

[57] Reich NH, Alsema EA, van Sark WGJHM, Turkenburg WC, Sinke WC. Greenhouse gas emissions associated with photovoltaic electricity from crystalline silicon modules under various energy supply options. Progress Photovolt Res Appl 2011;19(5):603–13.

[58] Yin A, Zhang Z, Jin X, Wang H, Zhang M, Wang H. Carbon emission analysis of two crystalline silicon components throughout the life cycle. IOP Conf Ser Earth Environ Sci 2022;983:012111.

[59] Leccisi E, Raugei M, Fthenakis V. The energy and environmental performance of ground-mounted photovoltaic systems—a timely update. Energies 2016;9(8):622.

[60] Nian V. Impacts of changing design considerations on the life cycle carbon emissions of solar photovoltaic systems. Appl Energy 2016;183:1471–87.

[61] Eskew J, Ratledge M, Wallace M, Gheewala SH, Rakkwamsuk P. An environmental life cycle assessment of rooftop solar in Bangkok. Thailand Renew Energy 2018;123:781–92.

[62] Energy Market Authority. Installed capacity & number of installations. 2023.

[63] Zhu R, Wong MS, You L, Santi P, Nichol J, Ho HC, et al. The effect of urban morphology on the solar capacity of three-dimensional cities. Renew Energy 2020;153:1111–26.

[64] Energy Institute. Statistical review of world energy. 2022.

[65] Todde G, Murgia L, Deligios PA, Hogan R, et al. Energy and environmental performances of hybrid photovoltaic irrigation systems in Mediterranean intensive and super-intensive olive orchards. Sci Total Environ 2019;651(2):2514–23.

[66] Grant CA, Hicks AL. Effect of manufacturing and installation location on environmental impact payback time of solar power. Clean Technol Environ Pol 2020;22:187–96.

[67] Xie M, Ruan J, Bai W, Qiao Q, Bai L, Zhang J, et al. Pollutant payback time and environmental impact of Chinese multi-crystalline photovoltaic production based on life cycle assessment. J Clean Prod 2018;184:648–59.

[68] Marimuthu C, Kirubakaran V. Carbon payback period for solar and wind energy project installed in India: a critical review. Renew Sustain Energy Rev 2013;23:80–90.

[69] de Wild-Scholten MM. Energy payback time and carbon footprint of commercial photovoltaic systems. Solar Energy Mater Solar Cells 2013;119:296–305.